Combined nonlinear effects for UV to visible wavelength generation in a photonic crystal fiber

Binbin Yan (颜玢玢)[1], Jinhui Yuan (苑金辉)[1,2,*], Xinzhu Sang (桑新柱)[1], Kuiru Wang (王葵如)[1], and Chongxiu Yu (余重秀)[1]

[1]*State Key Laboratory of Information Photonics and Optical Communications, Beijing University of Posts and Telecommunications, Beijing 100876, China*

[2]*Guangdong Provincial Laboratory of Nanophotonic Functional Materials and Devices, South China Normal University, Guangzhou 510006, China*

**Corresponding author: yuanjinhui81@163.com*

Received November 9, 2015; accepted March 4, 2016; posted online April 5, 2016

We experimentally study the combined nonlinear effects, including four-wave mixing, stimulated Raman scattering, soliton dynamics, and cross-phase modulation by coupling femtosecond pulses around 850 nm into the normal dispersion region near the zero-dispersion wavelength in the fundamental mode of a homemade silica photonic crystal fiber. The nonlinear optical dynamics at different stages are demonstrated, and the discrete ultraviolet (UV) to visible wavelengths widely separated from the pump wave are generated by the interaction of several nonlinear effects involved. The UV to visible wavelengths can be used as short pulse sources for multiphoton ionization, fluorescence spectroscopy, and biochemical imaging.

OCIS codes: 060.5295, 190.4370.

doi: 10.3788/COL201614.050603.

In the past few years, lots of studies have been explored for the generation of ultrashort optical pulses at the visible and ultraviolet (UV) wavelengths because they have important applications in basic physical and biochemical science such as multiphoton ionization, fluorescence spectroscopy, and biochemical imaging. Photonic crystal fibers (PCFs)[1–6] with controllable properties over dispersion and nonlinearity have opened a new phase in the development of nonlinear optics. They offer the ideal optical media for enabling some nonlinear optical processes to be used for converting pump pulses available from the existing lasers into the UV to visible wavelengths that are widely separated from the pump wave.

Supercontinuum (SC) generation involved in extremely wide spectral broadening results from the complex interaction between a series of nonlinear effects[7–14]. Although it is possible to obtain the discrete desired wavelengths through selectively filtering the generated SC, the efforts on extending the blue edge of the SC toward the UV to visible spectral region are demonstrated to be difficult, and the temporal width of the filtered wavelengths can be elongated along with the decreased output energy. Thus, the non-SC frequency upconversion techniques based on single four-wave mixing (FWM)[15–18] or soliton dynamics[19–22] are developed through controlling the initial nonlinear evolution of the pump pulses so as to suppress the SC generation. Generation of UV to visible wavelengths by FWM in a PCF requires that the wavelength of the pump pulses around 800 or 532 nm is close to but shorter than the zero-dispersion wavelength (ZDW) of the fundamental mode of a PCF with a core diameter of less than 2 μm. However, the PCF is difficult to draw, and it suffers from high propagation loss and damage at high incident power. Dispersive waves (DWs) during the soliton dynamics can also be used for generating UV to visible wavelengths in the small-core PCFs doped by rare earth elements[23], but the material preparation for the fiber preform is difficult and the effect of rare earth ions on the nonlinear optical process needs to be considered. Recently, the deep-UV DWs were generated in an Ar-filled hollow-core PCF (HC-PCF) with pressure-controlled dispersion, but the complex nonlinear optical property of Ar had a determined influence on the process of energy conversion[24]. Up to now, it was demonstrated that the generation of UV to visible wavelengths by a single nonlinear effect is difficult. Thus, the mutual effect of several nonlinear effects in PCFs at the early stage of SC generation has become the subject of some studies[25,26] that can be expected to solve the current problem. Hsieh *et al.* preliminarily studied the combined effect of Raman and parametric gain in the optical parametric process[25]. Kudlinski *et al.* demonstrated the combined FWM and Raman effects in a PCF[26]. However, the combined nonlinear dynamics involving three or more nonlinear effects have not yet been reported.

In this Letter, femtosecond pulses are coupled into the normal dispersion region near the ZDW in the fundamental mode of a homemade silica PCF, and the nonlinear optical processes referring to FWM, stimulated Raman scattering (SRS), soliton dynamics, and cross-phase modulation (XPM) are experimentally demonstrated. The discrete UV to visible wavelengths are efficiently generated by the combined nonlinear effects.

Figure 1 shows the group-velocity dispersion (GVD) curve of the fundamental mode. It is calculated with the multipole method (MPM) from the cross-sectional structure of the silica PCF with a core diameter as large

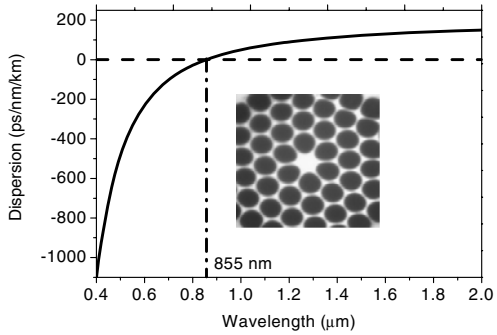

Fig. 1. GVD curve calculated for the fundamental mode with the ZDW of 855 nm, and the inset shows the cross-sectional structure of PCF used.

as 2.85 μm and a relative hole size of 0.91, as shown in the inset of Fig. 1. During the fabrication process, the silica material is first purified by the combined method of rectification and adsorption to greatly reduce the absorption losses induced by the chlorides, chlorine-hydrogen compounds, OH, metal ions, and metallic and nonmetallic oxides, and then the PCF is fabricated from the silica material by the stack and draw technology. The ZDW is located at 855 nm, so the PCF has a normal dispersion region at the pump wavelength of 850 nm used in the latter experiment.

The FWM as an elastic nonlinear effect requires the phase-matching condition to be satisfied. For the degenerate case, two pump photons at ω_p can generate a Stokes photon at the downshifted frequency ω_s and an anti-Stokes photon at the upshifted frequency $\omega_{\rm as}$; that is to say, $2\omega_p = \omega_s + \omega_{\rm as}$. In order to achieve efficient energy conversion, the phase mismatching induced by the silica material and waveguide structure requires compensation by the nonlinear ones through the relation[17,18]

$$\kappa = \beta(\omega_s) + \beta(\omega_{\rm as}) - 2\beta(\omega_p) + 2\gamma P = 0, \qquad (1)$$

where $\beta(\omega_s)$, $\beta(\omega_{\rm as})$, and $\beta(\omega_p)$ are the propagation constants of the Stokes, anti-Stokes, and pump wave, respectively, $\gamma = n_2\omega_0/cA_{\rm eff}$ is the nonlinear coefficient, $A_{\rm eff}$ is the effective mode area, and $n_2 = 2\times10^{-20}$ m^2/W is the nonlinear refractive index of the silica material.

As the pump energy is extended into the anomalous dispersion region, the soliton dynamics dominate the nonlinear optical process. The location of DWs can be governed by the phase-matching condition referring to the dispersion and nonlinear contribution[20,21]

$$\sum_{n\geq2}\frac{(\omega_{\rm DW}-\omega_p)^n}{n!}\beta_n(\omega_p) = \frac{\gamma P_p}{2}, \qquad (2)$$

where $\omega_{\rm DW}$ and ω_p are the central frequencies of DWs and pump pulses. β_n denotes the propagation constant's nth-order derivative taken at ω_p, and γ and P_p represent the nonlinear coefficient of the fiber and the peak power of the pump pulses, respectively. In this work, we have

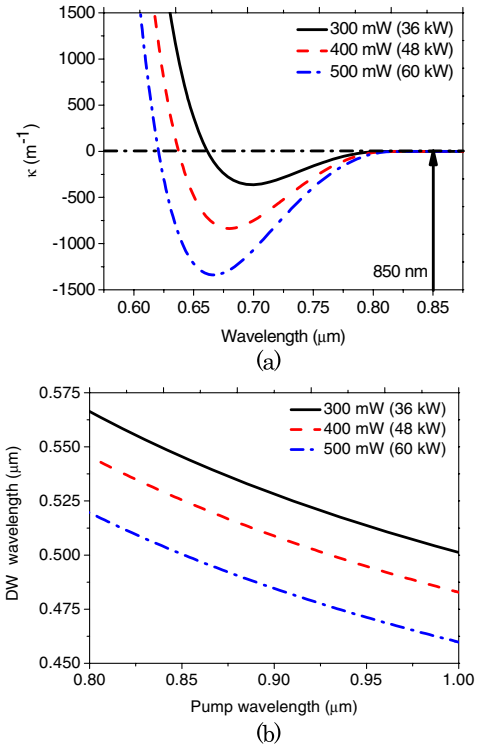

Fig. 2. (a) Phase-mismatching factor κ at the short wavelength in the fundamental mode of the PCF calculated as a function of wavelength when the pump pulses are centered at 850 nm and the input average power is increased from 300 to 400, and to 500 mW (the peak power of 36 to 48, and to 60 kW), the vertical arrow line corresponding to a pump wavelength of 850 nm and (b) the phase-matching condition between the DW and pump wavelengths for the same pump condition.

considered the Taylor expansion up to the fifth order ($n = 5$), and the corresponding dispersion coefficients are $\beta_2 = 1.2536$ ps^2/km, $\beta_3 = 0.3285\times10^{-2}$ ps^3/km, $\beta_4 = -0.9523\times10^{-6}$ ps^4/km, and $\beta_5 = 1.4257\times10^{-8}$ ps^5/km at the pump wavelength of 850 nm.

When pump pulses are centered at 850 nm and input average power is increased from 300 to 400, and to 500 mW (the peak power of 36 to 48, and to 60 kW), the phase-mismatching factor κ calculated from Eq. (1) is shown in Fig. 2(a). It can be seen that κ reaches zero at wavelengths of 661, 637, and 621 nm, which predicts that the anti-Stokes wave can be generated at these wavelengths widely separated from the pump wave. Moreover, the DW wavelengths are calculated as a function of the pump wavelengths by Eq. (2), as shown in Fig. 2(b).

The experimental setup used to test the PCF is shown in Fig. 3(a). The experiment is performed with a mode-locked Ti:sapphire laser (800 nm center wavelength, 120 fs pulse width, and 76 MHz repetition rate). The mode-locked state of the pump pulses is monitored by the oscilloscope, and an optical isolator is placed at the output end of the laser to prevent light from reflecting back into the laser system. The output pump beams are launched into a span of 160-cm-long PCF by using a 40× microscope objective with a coupling efficiency of

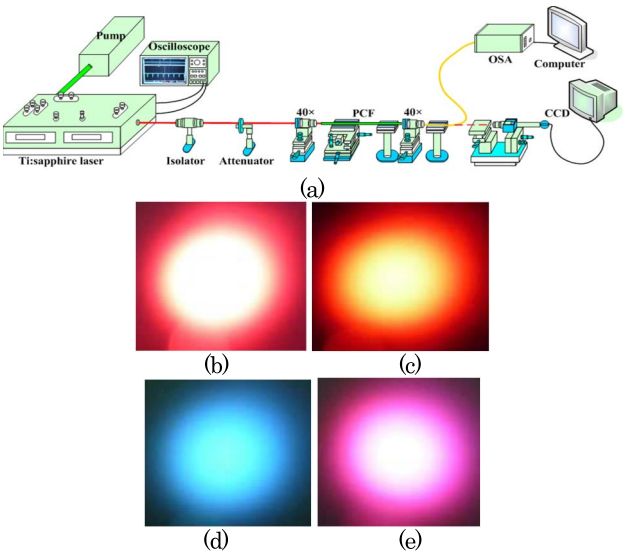

Fig. 3. (a) Experimental setup, and (b), (c), (d), and (e) show the observed output far fields at the wavelengths of 650, 620, 500, and 400 nm when the input average power of the pump pulses centered at 850 nm are kept at 500 mW, corresponding to the red, red-orange, green-blue, and pink-violet light, respectively.

66%, and the input average powers can be controlled with a variable attenuator. The coupling state of the incident light beams is monitored by the CCD. The fundamental mode can be excited by focusing the pump pulses onto the fiber face along the direction of the core central axis. The propagation loss is measured by the cutback method to be about 0.23 dB/m at 850 nm. The output spectra are directly observed by an optical spectrum analyzer (OSA, Avaspec-256) with a wavelength range of 200 to 1100 nm. Figures 3(b), 3(c), 3(d), and 3(e) show the output far fields observed by the CCD at wavelengths of 635, 620, 500, and 400 nm, respectively, when the wavelength and input average power of the pump pulses are kept at 850 nm and 500 mW, respectively. In the experiment, both the fiber length and pump pulse parameters are appropriately selected to study the early stage of SC generation. In addition, the Stokes waves and solitons generated at the near-infrared wavelengths will fall out of the spectral range of the OSA.

The evolution of the output spectra within the wavelength range of 200 to 1000 nm is measured for the input average powers $P_{\mathrm{av}} = 300$, 400, and 500 mW (the corresponding peak powers are 36, 48, and 60 kW), respectively, when the pump pulses at 850 nm are launched into the 160-cm-long fiber, as shown in Fig. 4(a). At the initial stage of the nonlinear optical process, because the pump wavelength is located in the normal dispersion region and close to the ZDW of the fundamental mode of the PCF, the FWM as a dominant nonlinear effect generates the anti-Stokes sidebands at wavelengths of 662, 636, and 620 nm due to the higher-order dispersion, which is consistent with the calculated results shown in Fig. 2(a). As the anti-Stokes wave energy is gradually enhanced along the propagation distance, its own Raman Stokes

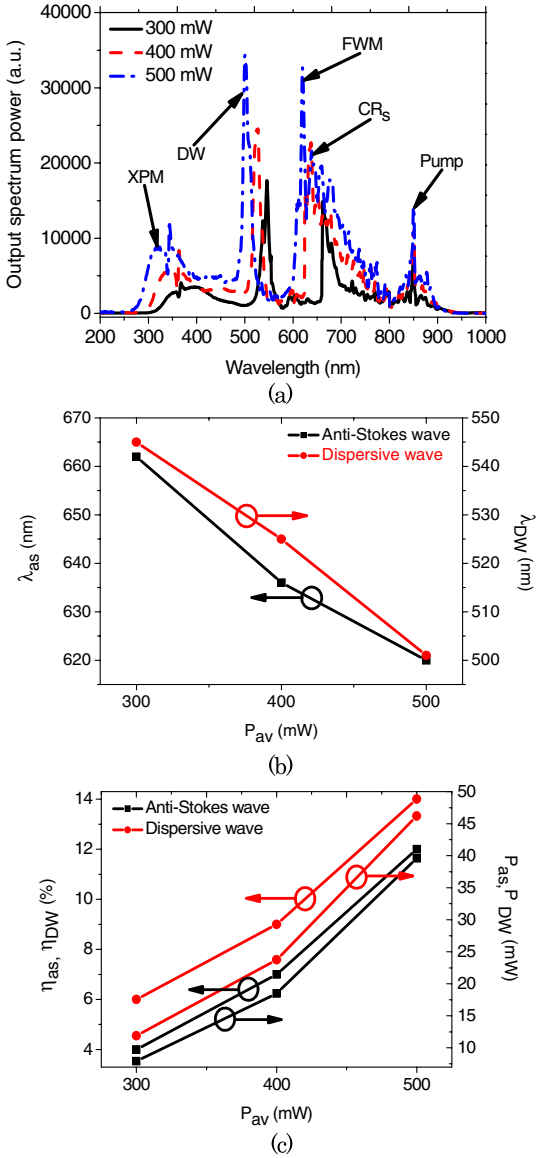

Fig. 4. (a) Observed output spectra when the input average power P_{av} of the pump pulses at 850 nm increases from 300 (black solid line), to 400 (red dashed line), and to 500 mW (blue dot-dashed line), (b) the anti-Stokes wave and DW wavelengths λ_{as} and λ_{DW} as a function of P_{av}, and (c) the conversion efficiencies η_{as} and η_{DW}, and the output powers P_{as} and P_{DW} of the anti-Stokes waves and DWs as a function of P_{av}.

orders at the longer wavelength side are generated especially for $P_{\mathrm{av}} = 500$ mW. Moreover, because the injected peak powers (36, 48, and 60 kW) are evidently higher than the that of the Raman threshold, the optical spectra of the pump pulses can be broadened asymmetrically on the leading and trailing edges through the Raman and self-phase modulation (SPM) effects. It is worth noting that there is no spectral overlap between the FWM and Raman spectra because the frequency shift of FWM relative to the pump wave is much larger than the Raman gain band. As part of the pump energy is extended into the anomalous dispersion region of the PCF, the soliton dynamics play an important role. The Raman solitons formed by the

interaction between the negative dispersion and the SPM occur to shift toward the longer wavelength. When the perturbation is induced by the higher-order dispersions during the redshift process, the resonant blueshifted DWs are generated at wavelengths of 545, 525, and 501 nm, respectively, agreeing well with the theoretical results shown in Fig. 2(b). At first, no interaction between the Raman solitons and DWs exists because of the large temporal separation induced by the group-velocity difference. During the further propagation, the faster Raman solitons slow down and are eventually caught up by the accelerating DW pulses. At this time, the Raman solitons trap part of the DW spectrum. The temporal overlap between them leads to the XPM, and new spectral components well separated from the DWs are generated at the shorter wavelengths below 400 nm. Also, it is evidenced from Figs. 3(b), 3(c), 3(d), and 3(e) that the related nonlinear processes occur in the spatial fundamental mode. The spectral broadening of the discrete UV to visible wavelengths in the normal dispersion region is believed to be due to dispersive and nonlinear effects.

Figure 4(b) shows the relationships between the anti-Stokes wave and DW wavelengths λ_{as}, λ_{DW}, and P_{av}. It can be seen from Fig. 4(b) that both λ_{as} and λ_{DW} are evidently shifted to the shorter wavelengths as P_{av} is increased from 300 to 400, and to 500 mW. The optical filters at different center wavelengths are used to separate out the anti-Stokes waves and DWs, and then a milliwatt power meter is used to measure the corresponding output powers. As shown in Fig. 4(c), when the coupling efficiency of 66% is achieved, the output powers of the anti-Stokes waves and DWs are measured to be 7.92, 18.48, and 39.6 mW; 11.88, 23.76, and 46.2 mW, respectively. The corresponding conversion efficiencies of η_{as} (the ratios between the power of anti-Stokes waves and the incident pump power) and η_{DW} (the ratios between the power of DWs and the incident pump power), are increased from 4 to 7, and to 12%; 6 to 9, and to 14%, respectively. In addition, considering the Manley–Rowe relation of photon conservation, the energies converted through the Raman and XPM effects are estimated to be no more than 15% for $P_{av} = 500$ mW. In the experiment, it is believed that the energy conversion processes by the combined nonlinear effects can be further enhanced through optimizing the pump pulse and PCF parameters to reduce the coupling and scattering loss from the fundamental to higher-order modes and depress the pulse walk-off between the pump wave and the anti-Stokes wave.

In conclusion, the interactions between several nonlinear effects including FWM, SRS, soliton dynamics, and XPM are experimentally studied by pumping in the normal dispersion region in the fundamental mode of a home-made PCF. The discrete UV to visible wavelengths are generated through the combined nonlinear processes. It can be expected that the UV to visible wavelengths generated can be used as short pulse sources for basic physical and biochemical science such as multiphoton ionization, fluorescence spectroscopy, and biochemical imaging.

This work was partly supported by the National Natural Science Foundation of China (Nos. 61307109, 61475023, and 61405014), the Beijing Youth Top-notch Talent Support Program (No. 2015000026833ZK08), the Natural Science Foundation of Beijing (No. 4152037), and the Fund of State Key Laboratory of Information Photonics and Optical Communications (BUPT), China (No. IPOC2015ZC06).

References

1. P. St. J. Russell, Science **299**, 358 (2003).
2. J. C. Knight, Nature **424**, 847 (2003).
3. P. St. J. Russell, J. Lightwave Technol. **24**, 4729 (2006).
4. L. Han, L. Liu, Z. Yu, H. Zhao, X. Song, J. Mu, X. Wu, J. Long, and X. Liu, Chin. Opt. Lett. **12**, 010603 (2014).
5. T. Wang, G. Liu, Y. Li, B. Yan, X. Chen, X. Sang, C. Yu, F. Xiao, and A. Kamal, Chin. Opt. Lett. **13**, 041404 (2015).
6. F. Tian, J. R. Kanka, and H. Du, Chin. Opt. Lett. **13**, 070501 (2015).
7. A. V. Husakou and J. Herrmann, Phys. Rev. Lett. **87**, 203901 (2001).
8. J. M. Dudley, G. Genty, and S. Coen, Rev. Mod. Phys. **78**, 1135 (2005).
9. L. He, B. Yang, X. Zhang, and L. Yu, Chin. Opt. Lett. **4**, 715 (2006).
10. A. Kudlinski and A. Mussot, Opt. Lett. **33**, 2407 (2008).
11. M. H. Frosz, P. M. Moselund, P. D. Rasmussen, C. L. Thomsen, and O. Bang, Opt. Express **16**, 21076 (2008).
12. L. Fang, J. Zhao, and X. Gan, Chin. Opt. Lett. **8**, 1028 (2010).
13. L. Zheng, X. Zhang, X. Ren, H. Ma, L. Shi, Y. Wang, and Y. Huang, Chin. Opt. Lett. **9**, 040601 (2011).
14. S. P. Stark, J. C. Travers, and P. St. J. Russell, Opt. Lett. **37**, 770 (2012).
15. D. Nodop, C. Jauregui, D. Schimpf, J. Limpert, and A. Tünnermann, Opt. Lett. **34**, 3499 (2009).
16. L. Lavoute, J. C. Knight, P. Dupriez, and W. J. Wadsworth, Opt. Express **18**, 16193 (2010).
17. Y. Chen, W. J. Wadsworth, and T. A. Birks, Opt. Lett. **38**, 3747 (2013).
18. J. H. Yuan, X. Z. Sang, Q. Wu, G. Y. Zhou, C. X. Yu, K. R. Wang, B. B. Yan, Y. Han, G. Farrell, and L. T. Hou, Opt. Lett. **38**, 5288 (2013).
19. P. K. A. Wai, C. R. Menyuk, Y. C. Lee, and H. H. Chen, Opt. Lett. **11**, 464 (1986).
20. I. Cristiani, R. Tediosi, L. Tartara, and V. Degiorgio, Opt. Express **12**, 124 (2004).
21. G. Q. Chang, L. J. Chen, and F. X. Kärtner, Opt. Lett. **35**, 2361 (2010).
22. J. H. Yuan, X. Z. Sang, C. X. Yu, Y. Han, G. Y. Zhou, S. G. Li, and L. T. Hou, IEEE Photon. Technol. Lett. **23**, 786 (2011).
23. X. B. Zhang, X. Zhu, L. Chen, F. G. Jiang, X. B. Yang, J. G. Peng, and J. Y. Li, Appl. Phys. B **111**, 273 (2013).
24. N. Y. Joly, J. Nold, W. Chang, P. Hölzer, A. Nazarkin, G. K. L. Wong, F. Biancalana, and P. St. J. Russell, Phys. Rev. Lett. **106**, 203901 (2011).
25. A. S. Y. Hsieh, G. K. L. Wong, S. G. Murdoch, S. Coen, F. Vanholsbeeck, R. Leonhardt, and J. D. Harvey, Opt. Express **15**, 8104 (2007).
26. A. Kudlinski, V. Pureur, G. Bouwmans, and A. Mussot, Opt. Lett. **33**, 2488 (2008).